Power Prediction of Wind Farm Considering the Wake Effect and its Boundary Layer Compensation

Zao Tang, *Member*, *IEEE*, Jia Liu, *Member*, *IEEE*, Jielong Ni, Jimiao Zhang, *Member*, *IEEE*, Pingliang Zeng, *Member*, *IEEE*, Pengzhe Ren, and Tong Su, *Member*, *IEEE*

***Abstract*—With significant expansion in wind farm capacity, wake disturbances from upstream wind turbines have emerged as a detrimental factor, adversely affecting the generated power of downstream units. However, the conventional power prediction models usually neglect the wake effect between adjacent wind turbines. To bridge this gap, this paper proposes a novel power prediction model that considers the wake effect and its boundary layer compensation, to enable joint spatial and temporal wind power prediction for wind farms. Firstly, a two-dimensional convolutional neural network is adopted to extract the key features and reconstruct wind power prediction data. Secondly, utilizing historical data, a long short-term memory algorithm is employed to investigate the correlation between elemental characteristics and wind data. Subsequently, a 3D-Gaussian Frandsen wake model that accounts for the wake effect and boundary layer compensation in wind farms is developed to precisely calculate the spatial wind speed distributions. Consequently, these distributions allow the power outputs of wind turbines in wind farms to be estimated more accurately via the rotor equivalent wind speed. Finally, several case studies are conducted to validate the effectiveness of the proposed method. The results demonstrate that the suggested approach yields favorable outcomes in predicting both wind speed and wind power.**

***Index Terms*—Wind farm, wind power prediction, wake effect, 3D-Gaussian Frandsen model, spatial-temporal distribution of wind speed.**

Received: December 30, 2023
Accepted: May 30, 2024
Published Online: November 1, 2024

Zao Tang, Jia Liu (corresponding author), Jielong Ni, and Pingliang Zeng (corresponding author) are with the Department of Automation, Hangzhou Dianzi University, Hangzhou 310038, China (e-mail: ztang@hdu.edu.cn; sjtu_lj@hdu.edu.cn; ny-lonciao@gmail.com; plz@hdu.edu.cn).

Jimiao Zhang is with the Department of Electrical and Computer Engineering, Rowan University, Glassboro 08028, USA (e-mail: zhangj@rowan.edu).

Pengzhe Ren is with the Jiaxing Power Supply Company of State Grid Zhejiang Electric Power Company, Jiaxing 314000, China (e-mail: renppz@126.com).

Tong Su is with the Department of Electrical and Computer Engineering, University of Connecticut, Storrs 06269, USA (e-mail: tongsu@uconn.edu).

DOI: 10.23919/PCMP.2023.000221

I. Introduction

Wind power, as an abundant renewable energy source, has emerged as the primary source of electricity supply. By 2021, the worldwide installed wind power capacity has reached 830 GW, while its share of global electricity usage is continuing to rise [1]. However, large-scale integration of wind power has posed an operational challenge to the existing electric power systems due to its high stochasticity. Furthermore, wake effects are more pronounced when preferred locations are densely packed with wind turbines. Consequently, the power production of wind farms can be considerably reduced, while the operating costs increased. One promising solution for ensuring efficiency, stability, and economy of the renewable electric power systems lies in accurate wind power prediction.

Recent research on wind power prediction has seen significant growth. The literatures on wind power prediction can be categorized into various models: physical models [2]–[4], conventional statistical models [5]–[7], artificial intelligence (AI) based models [8]–[10], [27], [29], and hybrid models [11], [12]. The physical models are the foundation of other kinds of methods, and usually take account of various meteorological factors and then map them to wind power [2], [3]. However, these models require accurate physical parameters and meteorological data, and are generally applied to a single wind turbine. The statistical models [5]–[7], [13] establish the relationship between wind power outputs and environmental factors, based on historical time series data. Markov model [5], Gaussian process regression [6] and other improved methods are commonly used to forecast wind farm outputs. These methods have been recognized for their high prediction accuracy. However, a limitation of the methods is that they treat the wind farm as a sin-

gular entity, thus overlooking the interactions among individual turbines. The AI-based models, such as the deep reinforcement learning [8] and deep belief network (DBN) [10], also utilize historical data to predict wind power, similar as statistical models. However, unlike statistical models, the AI-based approaches are entirely model-free, which are more scalable and versatile. To gain more accurate wind power prediction, it is crucial to consider both data characteristics and physical characteristics. Thus, by integrating the strengths of the above-mentioned models, the hybrid models show a better performance in predicting wind power.

When wind turbines use blades to extract kinetic energy from the wind, they also reduce the wind speed behind the rotor and swirl the air flow, which is called wake. The wake effect is becoming more noticeable with the increasing presence of wind farms. Reference [14] reveals that power loss due to wakes can reach 30% of the total power production. Since the physical models can better depict the wake effect and minimize the adverse impacts of the output restriction from the grid side, it is proposed to integrate these models with AI to enhance the prediction of wind power in wind farms. This hybrid method allows for both spatial and temporal characteristics of a wind farm. The proposed prediction model comprises two major parts: one is the wind speed time-series prediction model under external uncertainties, and the other is the spatial modeling of wind speed distributions under the wake effect.

The AI-based methods can be leveraged to accurately forecast wind speed time series. In [15], the convolutional neural networks (CNNs) are applied to wind power prediction. While feature extraction effectively reduces model complexity, this method is limited by its precision in prediction. References [16] and [17] employ the long short-term memory (LSTM) network, which significantly enhances the performance of long time series prediction thanks to its forget gate. Nevertheless, the improvement in prediction comes at the cost of longer training times. When CNN and LSTM are combined, multivariate time series (such as wind speed) can be accurately predicted. Meanwhile, physical modeling can be utilized to predict wind speed spatial distributions for wind farms. However, the wake effect on the downstream turbines needs to be accurately quantified. The Frandsen wake model [18] has found broad applications due to its simplicity in calculating wake-induced turbulence. While the original Frandsen model takes account of the law of momentum conservation, it neglects losses near the control surface as well as the compensating air flows [19]. Therefore, calibrations of this model are necessary in order to reduce errors in predicting the spatial wind speed distributions.

This paper presents a hybrid wind power prediction model with the wake effect and its boundary layer compensation considered. The proposed method forecasts the wind speed from both spatial and temporal perspectives, and predict the corresponding wind power. In the time-series prediction of wind speed, CNN and LSTM complement each other. Specifically, CNN is responsible for extracting key features, while LSTM focuses on prediction. For the spatial distributions of wind speed, a 3-D Frandsen model considering the wake effect is proposed. Compensation of the wake boundary layer is incorporated to enhance calculation accuracy. Lastly, the validity and effectiveness of the proposed method are verified by cases studies. The main contributions of this paper are as follows.

1) A spatiotemporal joint wind power prediction approach is proposed in this paper, and specifically, the utilization of CNN-LSTM for predicting wind speed patterns temporally, alongside the integration of the 3D Gaussian wake model to determine the spatial representation of wind speed distribution.

2) This paper introduces a refined 3D Gaussian wake model as an enhancement to the existing Frandsen wake model. Through the implementation of the 3D Gaussian wake model, a comprehensive representation of wind speed spatial distribution is achieved.

3) This paper introduces a novel approach employing the rotor equivalent wind speed model to compute wind turbine output, thereby enhancing the precision of prediction results. Besides, the method can amalgamate temporal wind speed prediction outcomes with the spatial distribution principles for integration of two elements.

The rest of this paper is structured as follows. Section II provides detailed information on the 2D-CNN-LSTM based wind speed prediction for a wind farm. Section III outlines the 3-D Frandsen wake model, factoring in boundary layer compensation, which can be employed to generate wind speed values in three dimensions. In Section IV, a power estimation based on the rotor equivalent wind speed method, which can be utilized to compute the power output of individual wind turbines as well as the entire wind farm, is presented. Section V presents a detailed case studies, and Section VI provides a summary of the conclusions.

II. 2D-CNN-LSTM-based Wind Speed Prediction

The wind speed prediction method framework, as illustrated in Fig. 1, comprises two components: 1) a feature extraction block based on 2D-CNN; and 2) a wind speed forecast block relying on the LSTM technology.

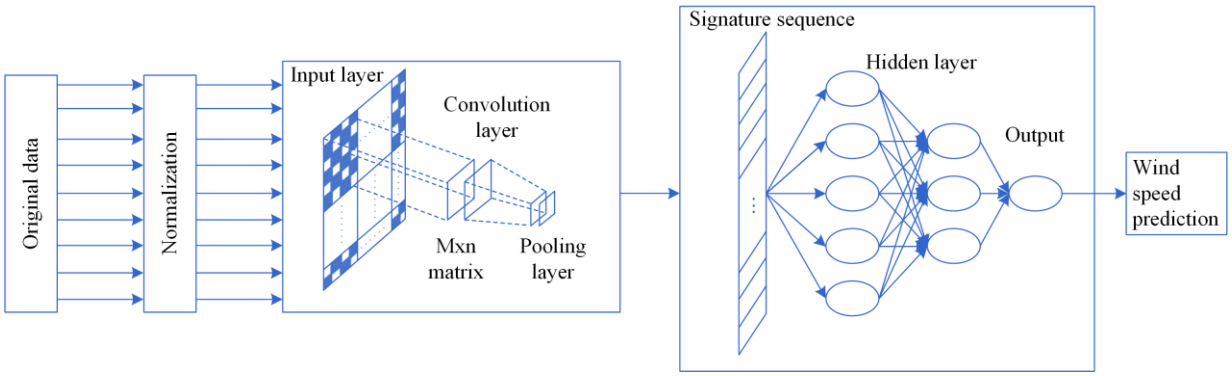

Fig. 1. The framework to predict wind speed based on the 2D-CNN-LSTM method.

A. 2D-CNN-based Feature Extraction Block

While technological advances in data collection allow more features to be used for prediction, the redundant features not only complicate model training and computation, but also diminish the prediction accuracy. CNNs can efficiently extract features. Through local connectivity and weight sharing, convolution, and pooling layers, CNNs perform feature extraction from the raw time series data and generate feature vectors for dimensionality reduction. The input features for the 2D-CNN feature extraction block include wind speed/direction, temperature, humidity, pressure, etc. Different features may have considerably different correlations with wind speed. Thus, transforming features to a similar scale will help improve the performance and training stability of the model [15]. Therefore, linear scaling is applied to the raw features related to the wind speed.

A 2D-CNN is adopted in this work due to its simplicity in feature extraction and data reconstruction. This 2D-CNN can efficiently capture temporal dependencies among each feature before feeding the extracted features into a LSTM network for relationship learning. The 2D-CNN model generates a set of feature sequences which serve as the input values for the LSTMs to facilitate the unfolding of wind power prediction training.

B. LSTM-based Wind Speed Prediction Block

LSTMs are a special type of recurrent neural network (RNN). An LSTM unit consists of an input gate, a forget gate, an output gate, and a memory cell that remembers past information. The vanishing gradient problem encountered in standard feedforward neural networks can be effectively addressed as LSTMs can work with long sequences of data [20]. The details of LSTMs are listed in [16] and [17].

The three gates in LSTMs jointly solve the vanishing gradient problem:

1) The input gate stores the wind speed x_t in the cell state;

2) The forget gate selectively discards redundant or non-essential information, and determines the extent of information to be removed from memory cell c_{t-1} for updating c_t;

3) The output gate chooses between the hidden state vector and the cell state vector before providing the appropriate input for the LSTM unit at the next time step.

III. 3-D Frandsen Wake Model Considering Boundary Layer Compensation

A. Frandsen Wake Model

In the Frandsen analytical model, a control volume is constructed around a wind turbine. In addition, it is assumed that the velocity deficit in the wake of the wind turbine follows a top-hat distribution, as shown in Fig. 2(a). This paper employs this model and conducts analysis of the wake effect. The wake velocity is presented as:

$$v_{\mathrm{w}} = v_0\left(\frac{1}{2}+\frac{1}{2}\sqrt{1-2C_{\mathrm{T}}\frac{r_0^2}{r_{\mathrm{w}}^2}}\right) \tag{1}$$

where v_0 is the incoming wind velocity and v_{w} is the wake velocity; C_{T} is the thrust coefficient; r_0 denotes the rotor radius; while r_{w} means the wake radius in the cross section with downstream distance x from the turbine.

The Frandsen model assumes a nonlinear expansion of the wake radius as:

$$r = \frac{1}{2}\left(\beta^{\frac{m}{2}}+k\frac{x}{2r_0}\right)^{\frac{1}{m}} r_0 \tag{2}$$

$$\beta = \frac{1-\alpha}{1-2\alpha} \tag{3}$$

where m is a shape factor that governs the order of the expansion; the wake radius r is directly proportional to one third of the distance x according to the shear flow theory in [21], therefore, m is usually chosen as 3; k is

the wake expansion coefficient which is typically chosen as 0.4; β governs the initial expansion rate; and α is a wake expansion coefficient.

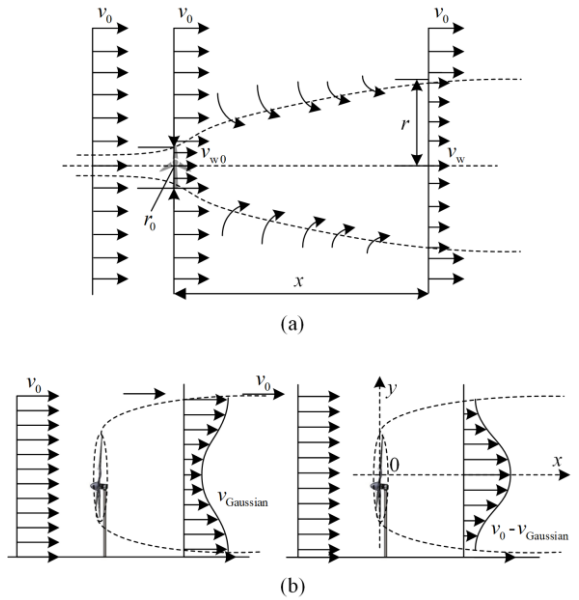

Fig. 2. Frandsen wake model. (a) Frandsen basic wake model and schematic diagram of boundary compensation. (b) Radial distribution and deficit of wake flow.

B. Compensation of Wake Boundary Layer

Frandsen assumes an equal velocity deficit in the cross-section of the wake. The model is derived by applying both mass and momentum conservation laws on a control volume located around the turbine. However, the air flow rate is neglected at the boundary of the control volume. In fact, the rotating blades of a wind turbine can cause significant turbulence to the atmospheric environment. Due to turbulent exchange of momentum in vortex shedding, the turbulent kinetic energy on the turbine outer surface will increase considerably (by around 40% in magnitude). In contrast, the air flow rate is relatively small around the turbine inner surface. Thus, the turbulent intensity is low in the wake straight behind the wind turbine. According to the turbulence theory, the free-stream flow and the turbulent flow will experience turbulences at the boundary layer. The interaction between the air flows inside and outside a control volume is elaborated as follows.

When the incoming air passes through the wind turbine blades, it undergoes an overall reduction in velocity with an expansion of the control volume. As part of the air flows out of the control volume boundary, there is a loss of incoming air flow for the control volume. When the air leaves behind the turbine, a pressure differential is resulted from the flow rate gradients inside and outside the control volume, thereby forcing the air outside to enter the control volume and to fill up the wake. Thus, the velocity inside the control volume will recover. Moreover, the pressure differential inside and outside the control volume decreases with an increase in the distance, and so will the air flow that enters the control volume. Theoretically, the amount of air will lower to zero at infinity, in which case the wake is fully recovered. The above process is termed as boundary layer compensation in this work.

Suppose that the external air flow compensates for the wake at an exponential decay rate. For the compensating air flow in the differential volume element dx with downstream distance x_r from the turbine, its proportion to the total air flow in the control volume is:

$$\mathrm{d}\bar{m} = \varphi\kappa \mathrm{e}^{-\kappa x_r}\mathrm{d}x \tag{4}$$

where φ is the compensation factor that governs how much of the external turbulent flow constitutes the compensating air flow in the control volume; κ is the compensation decay factor that governs the rate at which the external turbulent flow compensates for the control volume, in addition, the value of κ depends on the turbulence intensity I_0. Given the same terrain factors, the free-stream flow will have a stronger compensation effect on the wake for larger turbulence. Thus, the wake velocity recovers faster and κ takes a larger value. The relationship between κ and I_0 is expressed as [22]:

$$\kappa = \begin{cases} 0.4, I_0 < 10\% \\ 0.6, I_0 \geqslant 10\% \end{cases} \tag{5}$$

At infinity, the wake is fully compensated, i.e., an equilibrium is reached between the incoming and outgoing air flows for the control volume. The accumulated compensation ratio from the downstream distance x to infinity is derived as:

$$\bar{m} = \int_x^{\infty} \varphi\kappa \mathrm{e}^{-\kappa x}\mathrm{d}x = \varphi \mathrm{e}^{-\kappa x} \tag{6}$$

By applying the mass and momentum conservation laws and utilizing unified relative distances, it obtains:

$$\left(1-\varphi \mathrm{e}^{-\kappa\frac{x}{2r_0}}\right)\left[\rho\pi r_0^2 v_{w0} + \rho\pi(r_w^2 - r_0^2)v_0\right] = \rho\pi r_w^2 v_w \tag{7}$$

$$\left(1-\varphi \mathrm{e}^{-\kappa\frac{x}{2r_0}}\right)\left[\rho\pi r_0^2 v_{w0}^2 + \rho\pi(r_w^2 - r_0^2)v_0^2\right] = \rho\pi r_w^2 v_w^2 \tag{8}$$

where ρ represents the air density; and v_{w0} is the wake velocity at the fan. Combining and solving (1), (7) and (8) yield the initially calibrated Frandsen wake model:

$$v_w = v_0\sqrt{\left(1-\varphi \mathrm{e}^{-\kappa\frac{x}{2r_0}}\right)\left[1+(4\alpha^2-4\alpha)\frac{r_0^2}{r_w^2}\right]} \tag{9}$$

C. 3-D Gaussian Wake Model

Wind tunnel experiments and results of 3-D computational fluid dynamics (CFD) simulations both show that the actual cross-sectional wake velocities are not uniform and that the radial wake velocity deficit follows closely a Gaussian distribution, as shown in Fig. 2(b).

Inspired by these facts, we further calibrate the above modified Frandsen model with the assumption that the wake velocity deficit in the radial direction follows a Gaussian distribution. If the origin is chosen on the horizontal axis of the wind turbine, i.e., being zero, then the radial wake velocity deficit can be calculated as:

$$\Delta v = v_0 - v_{\mathrm{w}} = \frac{v_{\mathrm{sum}}}{\sqrt{2\pi}\sigma} \mathrm{e}^{-\frac{r^2}{2\sigma^2}} = \Delta v_{\max} \mathrm{e}^{-\frac{r^2}{2\sigma^2}} \tag{10}$$

Where σ is the standard deviation of the wake velocity deficit distribution; v_{sum} is the sum of wake velocities along the rotor diameter, i.e., $v_{\mathrm{sum}} = v_{\mathrm{w}} r_{\mathrm{w}}$; and $\Delta v_{\max}$ means the maximum velocity deficit at any downstream distance.

In a 3-D rectangular coordinate system, the x axis aligns with the wake centerline, which is also the horizontal axis of the turbine in ideal operating conditions. Additionally, the y axis is orthogonal to the x axis, and they are in the horizontal plane. The z axis is perpendicular to the x-y plane. If v is the velocity of the wake behind a wind turbine, then $\Delta v = v_0 - v$ represents the wake velocity deficit along the x axis.

Since the Gaussian distribution is assumed, the wake radius can be considered as infinitely large. As per the empirical rule [23]–[24], 99.73% of the wake velocity deficit observations will fall within the first three standard deviations $(\kappa - 3\sigma, \kappa + 3\sigma)$. Suppose 3σ is the wake boundary, i.e., $3\sigma = r_{\mathrm{w}}$, the standard deviation σ of the wake distribution is:

$$\sigma = \frac{1}{6}\left(\beta^{\frac{3}{2}} + \kappa \frac{x}{2r_0}\right)^{\frac{1}{3}} r_0 \tag{11}$$

Combining (9)–(11) and solving for $\Delta v_{\max}$ yield:

$$\Delta v_{\max} = \frac{6}{\sqrt{2\pi}} \left\{ 1 - \sqrt{\left(1 - \varphi \mathrm{e}^{-\kappa \frac{x}{2r_0}}\right)\left[1 + (4\alpha^2 - 4\alpha)\frac{r_0^2}{r_{\mathrm{w}}^2}\right]} \right\} v_0 \tag{12}$$

Furthermore, solving (10) and (11) yields the radial wake velocity deficit Δv:

$$\Delta v = \frac{6}{\sqrt{2\pi}} \left\{ 1 - \sqrt{\left(1 - \varphi \mathrm{e}^{-\kappa \frac{x}{2r_0}}\right)\left[1 + (4\alpha^2 - 4\alpha)\frac{r_0^2}{r_{\mathrm{w}}^2}\right]} \right\} \mathrm{e}^{-\frac{r^2}{2\sigma^2}} v_0 \tag{13}$$

Finally, the 3-D Gaussian wake model is derived as:

$$v_{\mathrm{w}} = \left\{ 1 - \frac{6}{\sqrt{2\pi}} \left\{ 1 - \sqrt{\left(1 - \varphi \mathrm{e}^{-\kappa \frac{x}{2r_0}}\right)\left[1 - \omega_T \frac{r_0^2}{r_{\mathrm{w}}^2}\right]} \right\} \mathrm{e}^{-\frac{r^2}{2\sigma^2}} \right\} v_0 \tag{14}$$

where

$$\omega_{\mathrm{T}} = 4\alpha - 4\alpha^2 \tag{15}$$

D. Wake Superposition Model

When multiple wind turbines are present in a wind farm, the wakes created by upstream turbines considerably affect the power generation and contribute to the fatigue loading of downstream turbines. It is crucial to take account of the cumulative wake effects when calculating incoming wind velocity for downstream turbines. As one of the most widely used superposition techniques, the sums of squares (SS) model is effective in approximating wind velocity in the areas where wake overlap occurs with each turbine. For N wind turbines, the model is expressed as:

$$\left(1 - \frac{v_{\mathrm{w-sum}}}{v_0}\right)^2 = \sum_{i=1}^{N} \left(1 - \frac{v_{\mathrm{w}j}}{v_0}\right)^2 \tag{16}$$

where $v_{\mathrm{w-sum}}$ denotes the wind velocity at a given location after considering the net contribution of overlapping wakes; and $v_{\mathrm{w}j}$ is the wake velocity for the jth turbine at the same location. If this location is not in the area of wake overlap, then $v_{\mathrm{w}j}$ should be equal to v_0.

Rearranging (16) leads to:

$$v_{\mathrm{w-sum}} = v_0 \left[1 - \sqrt{\sum_{i=1}^{N} \left(1 - \frac{v_{\mathrm{w}j}}{v_0}\right)^2} \right] \tag{17}$$

When factors such as geographical location are considered, it is easy to obtain accurate results of wind velocity at any location within a wind farm, thereby knowing the spatial distributions of the wind velocity.

To sum up, Section III details the 3D Frandsen wake model. Initially, the wind speed model is analyzed through the standard Frandsen wake model, denoted as v_{w} in (1). However, this model neglects the boundary compensation effect of wake. Consequently, we further explore the wake boundary effect on wind power, as illustrated in (4)–(8), leading to the initial calibration of Frandsen wake model, represented in (9). Since the velocity within the cross-section of a real wind turbine's wake area is not uniform, the radial wake velocity loss rate can be reasonably approximated by a Gaussian distribution. Hence, we assume that the velocity deficit in the wake's radial direction follows a Gaussian distribution, thereby refining the Frandsen model. This leads to the creation of a 3D-Frandsen wake model based on Gaussian distribution optimization, expressed in (14). The derivation process is outlined in (10)–(13). Lastly, considering the compensation effect of multiple wake boundaries on a wind turbine within a wind cluster, it becomes essential to overlay multiple wake actions on a single wind turbine, as discussed in Section III.D.

IV. Power Prediction Based on the 3-D Wake Model

A. Spatial-temporal Distribution of Wind Speed Considering Wind Farm Topology

While LSTM provides initial estimations of the incoming wind velocity for a wind farm, the spatial and temporal distributions of the wind speed are not uniform due to the wake effect, the turbulence effect, the stochastic nature of wind speed, etc. For the wind speed distributions within a cluster of wind turbines, the sequence in which the wind reaches each turbine needs to be considered. Thus, it is necessary to define a coordinate reference system using the wind directions, wherein the spatial locations of wind turbines can be specified.

Wind farms are usually located in regions with steady wind, while clusters of wind turbines are oriented to the prevailing wind, and therefore, there is little change in the wind direction in the short run. Since the yaw system is able to turn the wind turbine against variable wind, small variations in wind directions only have a negligible impact on the generated wind power. Nevertheless, spatial relationships between turbines will change as the wind direction varies. According to the wind farm topology and the direction of prevailing wind, a coordinate system can be created. When the wind direction experiences small changes, coordinate transformation is performed on the wind turbine coordinates, as:

$$\begin{cases} x' = x\cos\delta - y\sin\delta \\ y' = x\sin\delta + y\cos\delta \end{cases} \tag{18}$$

where (x, y) and (x', y') are the spatial coordinates of the turbine before and after the wind direction changes, respectively; δ refers to the angle between the current wind direction and the prevailing wind direction.

Given the extensive area covered by a wind farm, the delays cannot be ignored when modeling wind speed inside the wind farm. However, the short-term wind speed does not abruptly change while it continuously varies. Therefore, the prediction errors in wind farm power outputs due to non-uniform distribution of wind speed can be neglected. After the spatial coordinates of the wind farm are determined, the above 3D-Frandsen wake model is leveraged to depict the wind velocity at each point inside the wind farm, thus accurately characterizing the wind speed from spatial and temporal perspectives.

B. REWS Based Power Estimation

The prediction model derived above enables decoupling of each wind turbine and thus independent analysis of any individual one. Afterwards, the total power output of a wind farm can be obtained by summating the power output of each turbine.

Situated at the bottom of the neutral boundary layer, a wind farm typically harvests wind resources from 30 to 300 meters above the ground level. In this region, winds are not evenly distributed on the rotor because of the prevalent wind conditions such as wind shear, backing wind and turbulence. Traditional wind turbine power analyses typically consider only the incoming wind velocity at the turbine hub height. However, neglecting the fact of non-uniform wind speed distributions across the rotor will inevitably cause errors in subsequent analyses. The rotor equivalent wind speed (REWS) method [25] averages the weighted wind speed over the rotor's swept area and provides a more accurate estimate of the wind speed that corresponds to the kinetic energy flux passing through the rotor. In this paper, the power curves of wind turbines are optimized based on the REWS, which is defined as:

$$v_{\mathrm{rs}} = \left(\sum_{i=1}^{n} v_i^3 \frac{S_i}{S_0} \right)^{\frac{1}{3}} \tag{19}$$

where n represents the number of available measurement heights; v_{rs} is the REWS; v_i is the average wind speed measured at height i; S_i is the area of the ith segment; while S_0 refers to the total area swept by the rotor. An illustration is provided in Fig. 3.

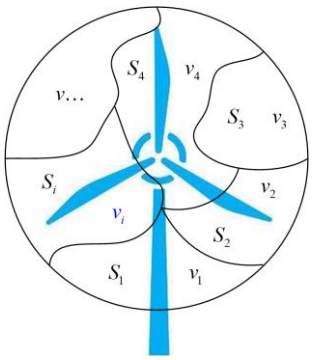

Fig. 3. Wind velocity distribution on the turbine surface.

When the incoming wind velocity is accounted, the REWS method can characterize the air flows more accurately and result in improved precision in wind power prediction. The equations related to the REWS method are summarized as:

$$v_{\mathrm{rs}} = \left(\sum_{i=1}^{n} v_i^3 \frac{S_i}{S_0} \right)^{\frac{1}{3}} \tag{20}$$

$$P = 2\rho S_0 v_{\mathrm{rs}}^3 \alpha (1-\alpha)^2 \tag{21}$$

where P is the power generated by the fan.

C. Proposed Method for Predicting Power in Wind Farms

To enhance the precision of wind farm power prediction, a three-step methodology is employed, as shown in Fig. 4. Firstly, CNN-LSTM technology is

utilized to predict the wind speed within the wind farm. The second step involves employing the 3D-frandsen wake model to recalculate the wind speed distributions in 3D space and re-evaluate the wind speed statistics for each wind turbine, based on the wind speed predictions made in the first step. Lastly, the REWS method is utilized to determine the wind speed for each turbine, thereby enabling the calculation of equivalent power. This approach results in a more accurate estimation of the wind farm's power output, as a result of accurate wind speed data obtained from varied locations within the wind farm.

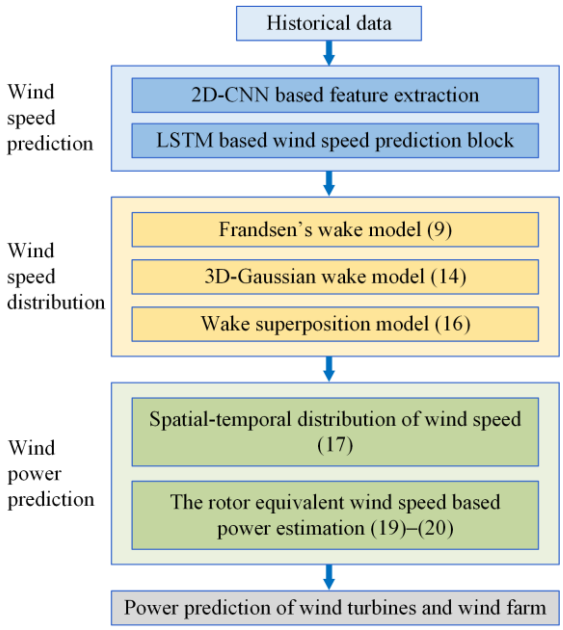

Fig. 4. Flowchart of the proposed method's procedure.

V. Case Studies

A. Datasets and Performance Measures

To validate the accuracy and effectiveness of the proposed wind power prediction approach, two case studies are conducted. Firstly, the historical datasets from a practical wind farm are utilized to test the wind speed prediction accuracy of the modified hybrid CNN-LSTM model. The supervisory control and data acquisition (SCADA) measures and records wind farm data at 10-minute intervals. The second case study compares the power outputs of the wind farm. The irregular layout with turbine displacements used by Vestas [26] is adopted in this paper. Based on the proposed 3D wake model and the predicted wind speed, the REWS for each turbine is used to calculate the wind power. Hence, the power outputs of each wind turbine and the entire wind farm are obtained.

B. Wind Speed Prediction for Wind Farms

To corroborate the superior performance of the proposed hybrid CNN-LSTM model, comparisons are made with other existing prediction models. The proposed method is the hybrid CNN-LSTM model that takes both historical data and numerical weather prediction (NWP) data as inputs, while another method defined as CL2, is the CNN-LSTM model, which only relies on historical data. The autoregressive integrated moving average (ARIMA) model and the RNN model are also considered. Different error metrics in (22)–(25) are calculated for a prediction horizon of 3 hours with 10-mintue steps. The results are shown in Table I.

Four common metrics are the root mean square errors (RMSE), mean absolute error (MAE), normalized root mean squared error (NRMSE), and normalized mean absolute error (NMAE), given as follows:

$$I_{\mathrm{RMSE}} = \sqrt{\frac{1}{n}\sum_{i=1}^{N}(x_i - \hat{x}_i)^2} \tag{22}$$

$$I_{\mathrm{MAE}} = \frac{1}{n}\sum_{i=1}^{N}(|x_i - \hat{x}_i|) \tag{23}$$

$$I_{\mathrm{NRMSE}} = \sqrt{\frac{1}{n}\sum_{i=1}^{N}(x_{ni} - \hat{x}_{ni})^2} \tag{24}$$

$$I_{\mathrm{NMAE}} = \frac{1}{n}\sum_{i=1}^{N}(|x_{ni} - \hat{x}_{ni}|) \tag{25}$$

where x_i and $\hat{x}_i$ are the actual and measured values, respectively; whereas x_{ni} and $\hat{x}_{ni}$ are their respective values after normalization.

TABLE I
Comparisons of Various Prediction Methods

Model	I_{RMSE}	I_{MAE}	I_{NRMSE}	I_{NMAE}
The proposed method	1.305	0.973	8.702	6.491
CL2	1.399	1.026	9.320	6.843
LSTM	1.727	1.288	11.516	8.590
ARIMA	1.768	1.301	11.791	8.658
RNN	2.039	1.508	13.593	10.091

Table I indicates that the prediction accuracy can be improved to some extent by incorporating NWP data. Meanwhile, it is observed that the CNN-LSTM model achieves better prediction performance than other models. In contrast, RNN has the worst prediction performance in terms of all the metrics, particularly when the distance becomes longer. This is because the explicit mechanism to forget has limited the RNN's predictive abilities.

C. Wind Power Prediction for Wind Farms

Two scenarios are analyzed to evaluate the performance of different models in predicting wind power. In Case 1, the predicted wind power for a wind farm with only two perpendicular turbines are compared. In Case 2, the wind farm under consideration has the same displacement layout as in the Vestas research, which is illustrated in Fig. 5.

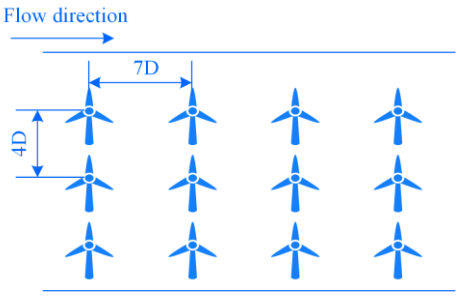

Fig. 5. Layout diagram of the wind farm.

In practical wind farms, the vertical distance between two wind turbines is typically 4 to 8 times the rotor diameter (D), while the horizontal distance is about 3 to 5 times the rotor diameter [28]. This paper assumes the rotor diameter of 60 m, with the vertical and horizontal distances of 7Ds and 4Ds, respectively. Table II shows the wind speeds (input) and the wind power (output) for different prediction models in the two cases.

TABLE II
WIND POWER COMPARISON OF DIFFERENT CASES

Case	Variables	Case 1	Case 2
Without wake model	v	1	1
	P	1	1
Park wake model [30]	v	0.916 58	0.847 08
	P	0.789 18	0.629 76
Frandsen wake model	v	0.969 64	0.935 21
	P	0.914 36	0.822 74
The proposed model	v	0.966 88	0.932 72
	P	0.907 10	0.816 91
The actual value	v	0.947 55	0.919 667
	P	0.888 95	0.805 475

It can be observed from Table II that the wind power extracted by the turbines decrease if the wake effect is considered, thus reducing the power output of the wind farm. In addition, both the average wind speeds and power outputs due to the Park wake model [30] and the proposed 3D-Frandsen wake model are reduced. However, the results from the Park wake model exhibit a more pronounced reduction. This is because it does not consider the fact that the air flow outside the control volume compensates for the wake so the wake effect on the downstream turbines is overestimated. Furthermore, errors in the wind farm power prediction can be primarily attributed to two factors, i.e., the error in wind speed prediction by the CNN-LSTM and the error in calculating wind speed redistribution, which arises from using distinct models. The study indicates that the modified calculation of wind speed distribution, utilizing the 3D-frandsen wake model and the REWS method, yields results that are markedly more accurate and closer to the actual values than the other methods. As demonstrated in Table III, the errors of power prediction in Case 1 and Case 2 are 2.041% and 1.420%, respectively, which are remarkably close to the true value. Comparing the 3D-Frandsen wake model to the standard Frandsen wake model, there is only a small variation in the average input wind speeds and average wind power outputs. However, the 3D-Frandsen wake model accounts for the uneven distribution of wind speed in the wake area. Hence, it shows enhanced precision and performance, especially for wind farms with a complex layout.

Moreover, a comparison of the results between Case 1 and Case 2 indicates that the wake effect within a wind farm has a higher impact on the total power output as the wind farm grows in size.

To further analyze the wake effect from the upstream wind turbines on those sitting downstream, the wind speed attenuation factor ω_b and the power attenuation factor ω_p are defined as follows:

$$\omega_b = \frac{v_0 - v_{in-w}}{v_0} \times 100\% \tag{26}$$

$$\omega_P = \frac{P_0 - P_w}{P_0} \times 100\% \tag{27}$$

where v_{in-w} and P_w refer to the respective input wind speed and power when the wake effect is considered, whereas v_0 and P_0 are the corresponding quantities when the wake effect is not considered.

Figure 6 depicts the wake attenuation of the incoming wind flow within a cross section at different coaxial distances when the 3D-Frandsen wake model is applied to Case 2. As seen, the wind speed drops when the natural wind passes through the wind turbine. A comparison of Figs. 6(a)–(c) shows a superposition of the decays, meaning that the wind turbines in the back rows see a further decrease in wind velocity. However, Figs. 6(d)–(f) indicate that the boundary layer compensation can mitigate the decaying effects. The wind velocity at infinity will return to the value of the incoming wind velocity.

Using the REWS method, the equivalent wind speeds for wind turbines in different rows are obtained. Then, the wind speed and power attenuation factors can be readily calculated, as presented in Table III. It shows that the natural wind suffers from a reduction in speed as it passes through the wind turbines in the front rows, hence affecting the operating conditions of the wind turbines in the back rows. Due to the superposition of wake, the speed of incoming wind reduces whenever it passes a row. The available wind speed to the downstream wind turbines falls considerably, while the power output of downstream wind turbines can decline by up to 30%.

TABLE III
ATTENUATION FACTORS UNDER THE CONDITIONS OF CASE 2

Wind turbine row number	ω_p	$\Delta\omega_p$ (%)
2	6.62	18.58
3	9.15	25.01
4	11.06	29.64

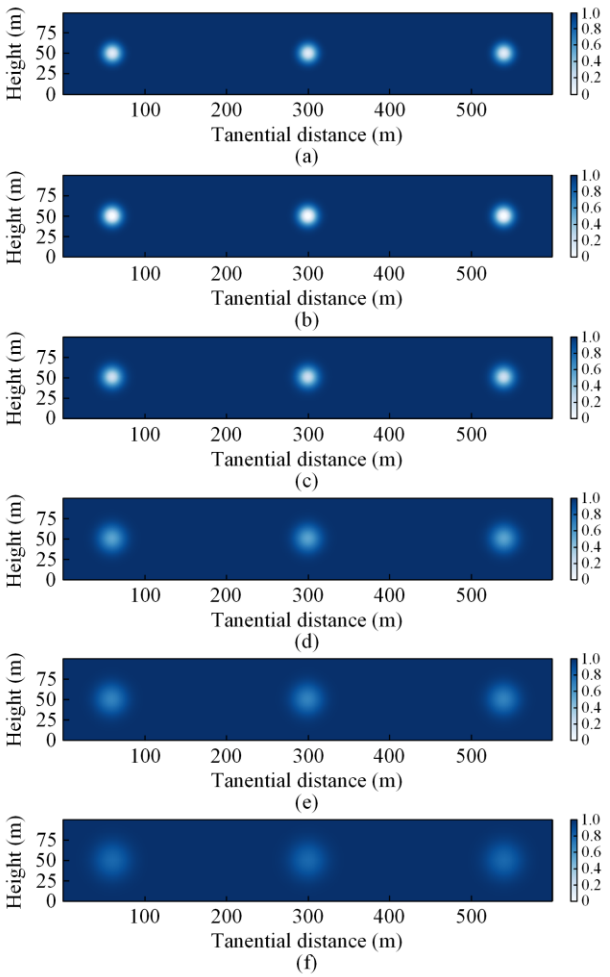

Fig. 6. Wake attenuation at different coaxial distances. (a) Wind speed section at 1100 m axial distance. (b) Wind speed section at 1500 m axial distance. (c) Wind speed section at 2000 m axial distance. (d) Wind speed section at 3000 m axial distance. (e) Wind speed section at 4000 m axial distance. (f) Wind speed section at 6000 m axial distance.

VI. Conclusion

In this paper, a method for predicting the power outputs of wind farms is proposed, which considers the wake effect and its boundary layer compensation. The proposed method is composed of three distinct blocks. In the first block, the incoming wind velocity is predicted by an improved hybrid CNN-LSTM model. The second block constructs a joint spatial and temporal wind speed distribution model by considering the wake effect. The third block focuses on predicting the total power output of the wind farm. Additionally, the topology information of the turbine cluster under varying incoming wind directions is incorporated into the analysis, and thus, it enables a decoupled power analysis of each individual turbine and leads to an aggregate prediction of the wind farm's total power output. In summary, the cases studies have demonstrated that:

1) The proposed hybrid 2D-CNN-LSTM, which incorporates historical and NWP data, achieves higher precision in short-term wind prediction.

2) The wake effect on turbines is intensified by wake overlap, especially as the distance downstream increases. This is because wind turbines located in the wake area exhibit reduced performance, with downstream turbines experiencing a decrease in power outputs. This reduction negatively impacts overall wind power generation.

3) The REWS based on the 3-D Frandsen wake model, along with the calculated wind power, provide more accurate representations of practical operating conditions for each turbine within the cluster.

However, the model presented in this paper omits the factor of pitch angle control in wind turbine operations. Thus, to further enhance the precision of dynamic wind power prediction, future research will explore the aspect of pitch angle control more comprehensively. This would allow to integrate this critical factor and significantly improve the overall accuracy of the analysis.

Acknowledgment

Not applicable.

Authors' Contributions

Zao Tang: full-text writing and the construction of the paper framework, software and simulations. Jia Liu: full-text revise. Jielong Ni: software and simulations. Jimiao Zhang: full-text revise. Pingliang Zeng: funding. Pengzhe Ren and Tong Su: full-text revise. All authors read and approved the final manuscript.

Funding

This work is supported by the Zhejiang Science and Technology Program (No. 2023C01142), the National Natural Science Foundation of China (No. 52207085 and No. 52407090), Zhejiang Provincial Natural Science Foundation of China (No. LY24E070006), and China Postdoctoral Science Foundation (No. 2024M750462).

Availability of Data and Materials

Not applicable.

Authors' Information

Zao Tang received the B.S. degree and Ph.D. degree in the College of Electrical Engineering, Sichuan University, Chengdu, China, in 2016 and 2021, respectively. She has been a visiting scholar with the Stevens Institute of Technology, Hoboken, NJ, USA during 2019–2020 and now She is a research lecture in the Department of Automation, Hangzhou Dianzi University. Her current research interests are the optimal planning and operation of power systems.

Jia Liu received the B.S. and Ph.D. degrees in electrical engineering from Tianjin University, Tianjin, China, and Shanghai Jiao Tong University, Shanghai, China, in 2014 and 2019, respectively. He was a post-doctoral in Zhejiang University, Hangzhou, China, and a visiting scholar in Cardiff University, Cardiff, U.K. He is currently an associate professor in Hangzhou Dianzi University, Hangzhou, China. His main research interests are planning, assessment and operation of power and energy systems, distributed optimization in transmission and distribution networks.

Jielong Ni received the B.S. degree in the Department of Automation from Hangzhou Dianzi university, in 2023. Now, he is an engineer in Zhejiang Company.

Jimiao Zhang received the B.Eng. degree in computer engineering from the Guangdong University of Foreign Studies in 2012, the M.Eng. degree in electric engineering from Chongqing University, China, in 2015, and the Ph.D. degree in electrical and computer engineering from Rowan University, NJ, USA, in 2023, where he is currently a research associate with the Electrical and Computer Engineering Department. From 2015 to 2017, he worked as a transmission line engineer with the State Grid Chongqing Electric Power Company. His research interests include operation and control of electrical distribution systems, renewable energy generation, and integration.

Pingliang Zeng is a professor at Hangzhou Dianzi University, Hangzhou, China. He is a chartered engineer (CEng), fellow of the IET, and a member of IEC TC122 and TC8. He obtained his bachelor and Ph.D. degrees, both in Electrical Engineering, respectively from Huazhong University of Science and Technology, China, in 1984, and Strathclyde University, UK, in 1990. Upon attaining doctorate degree, he joined National Grid Company (NGC), UK, where he held a number of important positions including system operator incentives and strategy manager, and network design manager. In 2012, he joined China Electric Power Research Institute as the chief expert in power system analysis and planning, where he led a research team undertaking a number of key projects including National High Technology Development ("863" Plan), SGCC special projects, and key Sino-UK joint research projects funded by National Natural Science Foundation of China on integration of EV and energy storage in power systems. He joined Hangzhou Dianzi University in August 2017. He has published one book and about 100 academic papers. His current research interests include power system planning under uncertainty, system operations, and renewable energy.

Pengzhe Ren received the B.Sc. degree from Northeast Electric Power University, Jilin, China, in 2019 and the M.Sc. degree from Sichuan University, Chengdu, China, in 2022, both in electrical engineering. His research interests include distribution network state estimation and distribution network planning.

Tong Su received the B.Sc. and M.S. degrees in electrical engineering from from Sichuan University, Chengdu, China, in 2019 and 2022, respectively. Since 2022, he has been working toward the Ph.D. degree from the University of Connecticut, Storrs, CT, USA. His research interests include power system dynamics and stability control with inverter-based resources, machine learning and optimization.

REFERENCES

[1] O. Summerfield-Ryan and S. Park, "The power of wind: the global wind energy industry's successes and failures," *Ecological Economics*, vol. 210, Aug. 2023.

[2] Y. Zhou, Q. Zhai and L. Wu, "Optimal operation of regional microgrids with renewable and energy storage: solution robustness and nonanticipativity against uncertainties," *IEEE Transactions on Smart Grid*, vol. 13, no. 6, pp. 4218-4230, Nov. 2022.

[3] K. Bakker, K. Whan, and W. Knap *et al.*, "Comparison of statistical post-processing methods for probabilistic NWP forecasts of solar radiation," *Solar Energy*, vol. 191, pp. 138-150, Oct. 2019.

[4] Z. Wang, W. Wang, and C. Liu *et al.*, "Probabilistic forecast for aggregated wind power outputs based on regional NWP data," *The Journal of Engineering*, vol. 2017, no. 13, pp. 1528-1532. Dec. 2017.

[5] Y. Cheng and S. Li, "Fuzzy time series forecasting with a probabilistic smoothing hidden Markov model," *IEEE Transactions on Fuzzy Systems*, vol. 20, no. 2, pp. 291-304, Apr. 2012.

[6] Y. Liu, J. Li, and W. Guan *et al.*, "Probabilistic prediction of wind power based on Gaussian process regression," in *2021 IEEE 4th International Conference on Automation, Electronics and Electrical Engineering (AUTEEE)*, Shenyang, China, Nov. 2021, pp. 34-38.

[7] X. Liu, X. Pu, and J. Li *et al*. "Short-term wind power prediction of a VMD-GRU based on Bayesian optimization," *Power System Protection and Control*, vol. 51, no. 21, pp. 158-165, Nov. 2023. (in Chinese)

[8] D. Cao, W. Hu, and X. Xu *et al.*, "Deep reinforcement learning based approach for optimal power flow of distribution networks embedded with renewable energy and storage devices," *Journal of Modern Power Systems and Clean Energy*, vol. 9, no. 5, pp. 1101-1110, Sept. 2021.

[9] B. Yang, B. Liu, and H. Zhou *et al*., "A critical survey of technologies of large offshore wind farm integration: summary, advances, and perspectives," *Protection and Control of Modern Power Systems*, vol. 7, no. 2, pp. 1-3, Apr. 2022.

[10] H. Z. Wang, G. B. Wang, and G. Q. Li *et al*., "Deep belief network based deterministic and probabilistic wind speed forecasting approach," *Applied Energy*, vol. 182, pp. 80-93, Nov. 2016.

[11] J. Xu, Z. Xiao, and Z. Lin *et al*., "System bias correction of short-term hub-height wind forecasts using the Kalman

filter," *Protection and Control of Modern Power Systems*, vol. 6, no. 4, pp. 1-9, Oct. 2021.

[12] Z. Zhu, K. W. Chan, and S. Xia *et al*., "Optimal bi-level bidding and dispatching strategy between active distribution network and virtual alliances using distributed robust multi-agent deep reinforcement learning," *IEEE Transactions on Smart Grid*, vol. 13, no. 4, pp. 2833-2843, Jul. 2022.

[13] Z. Cao, C. Wan, and Z. Zhang *et al*., "Hybrid ensemble deep learning for deterministic and probabilistic low-voltage load forecasting," *IEEE Transactions on Power Systems*, vol. 35, no. 3, pp. 1881-1897, May 2020.

[14] A. E. Feijoo, J. Cidras, and J. L. G. Dornelas, "Wind speed simulation in wind farms for steady-state security assessment of electrical power systems," *IEEE Transactions on Energy Conversion*, vol. 14, no. 4, pp. 1582-1588, Dec. 1999.

[15] H. Wang, G. Li, and G. Wang *et al*., "Deep learning-based ensemble approach for probabilistic wind power forecasting," *Applied Energy*, vol. 188, pp. 56-70, Feb. 2017.

[16] H. Zhang, L. Zhao, and Z. Du, "Wind power prediction based on CNN-LSTM," in *2021 IEEE 5th Conference on Energy Internet and Energy System Integration (EI2)*, Taiyuan, China, Oct. 2021, pp. 3097-3102.

[17] B. Zhou, X. Ma, and Y. Luo *et al.*, "Wind power prediction based on LSTM networks and nonparametric Kernel density estimation," *IEEE Access*, vol. 7, pp. 165279-165292, Nov. 2019.

[18] R. J. Barthelmie, G. C. Larsen, and S. T. Frandsen *et al.*, "Comparison of wake model simulations with offshore wind turbine wake profiles Measured by Sodar," *Journal of Atmospheric and Oceanic Technology*, vol. 23, no. 7, pp. 888-901, Jul. 2006.

[19] P. Argyle, S. Watson, and C. Montavon *et al.*, "Modelling turbulence intensity within a large offshore wind farm," *Wind Energy*, vol. 21, no. 12, pp. 1329-1343, Jul. 2018.

[20] Z. Yang, X. Peng, and P. Wei *et al.*, "Short-term wind power prediction based on CEEMDAN and parallel CNN-LSTM," in *2022 IEEE/IAS Industrial and Commercial Power System Asia (I&CPS Asia)*, Shanghai, China, Jul. 2022, pp. 1166-1172.

[21] H. Tennekes and J. L. Lumley, "Boundary-free shear flows," in *A First Course in Turbulence*, Cambridge, UK: M.I.T., 1972, pp: 104-145.

[22] L. P. Chamorro and F. Porté-Agel, "A wind-tunnel investigation of wind-turbine wakes: boundary-layer turbulence effects," *Boundary-Layer Meteorol*, vol. 132, no. 1, pp. 129-149, Jul. 2009.

[23] T. Su, J. Zhao, and X. Chen, "Deep sigma point processes-assisted chance-constrained power system transient stability preventive control," *IEEE Transactions on Power Systems*, vol. 39, no. 1, pp. 1965-1978, Jan. 2024.

[24] J. W. Park, A. Tumanov, and A. Jiang *et al*., "3Sigma: distribution-based cluster scheduling for runtime uncertainty," in *Proceedings of the Thirteenth EuroSys Conference*, Porto, Portugal, Apr. 2018, pp. 1-17.

[25] Y. Liu, Y. Qiao, and S. Han *et al*., "Rotor equivalent wind speed calculation method based on equivalent power considering wind shear and tower shadow," *Renewable Energy*, vol. 172, pp. 882-896, Jul. 2021.

[26] M. H. Vested, N. Hamilton, and J. N. Sørensen *et al*., "Wake interaction and power production of variable height model wind farms: 5th International Conference on The Science of Making Torque from Wind 2014," *Journal of Physics: Conference Series*, vol. 524, no. 1, Jun. 2014.

[27] T. Su, Y. Liu, and J. Zhao *et al*., "Probabilistic stacked denoising autoencoder for power system transient stability prediction with wind farms," *IEEE Transactions on Power Systems*, vol. 36, no. 4, pp. 3786-3789, Jul. 2021.

[28] C.-H. Moeng, "A large-eddy-simulation model for the study of planetary boundary-layer turbulence," *Journal of the Atmospheric Sciences*, vol. 41, no. 13, pp. 2052-2062, Jul. 1984.

[29] T. Su, J. Zhao, and Y. Pei *et al*., "Probabilistic physics-informed graph convolutional network for active distribution system voltage prediction," *IEEE Transactions on Power Systems*, vol. 38, no. 6, pp. 5969-5972, Nov. 2023.

[30] T. Göçmen, P. van der Laan, and P. E. Réthoré *et al*., "Wind turbine wake models developed at the technical university of Denmark: a review," *Renewable and Sustainable Energy Reviews*, vol. 60, pp. 752-769, Jul. 2016.